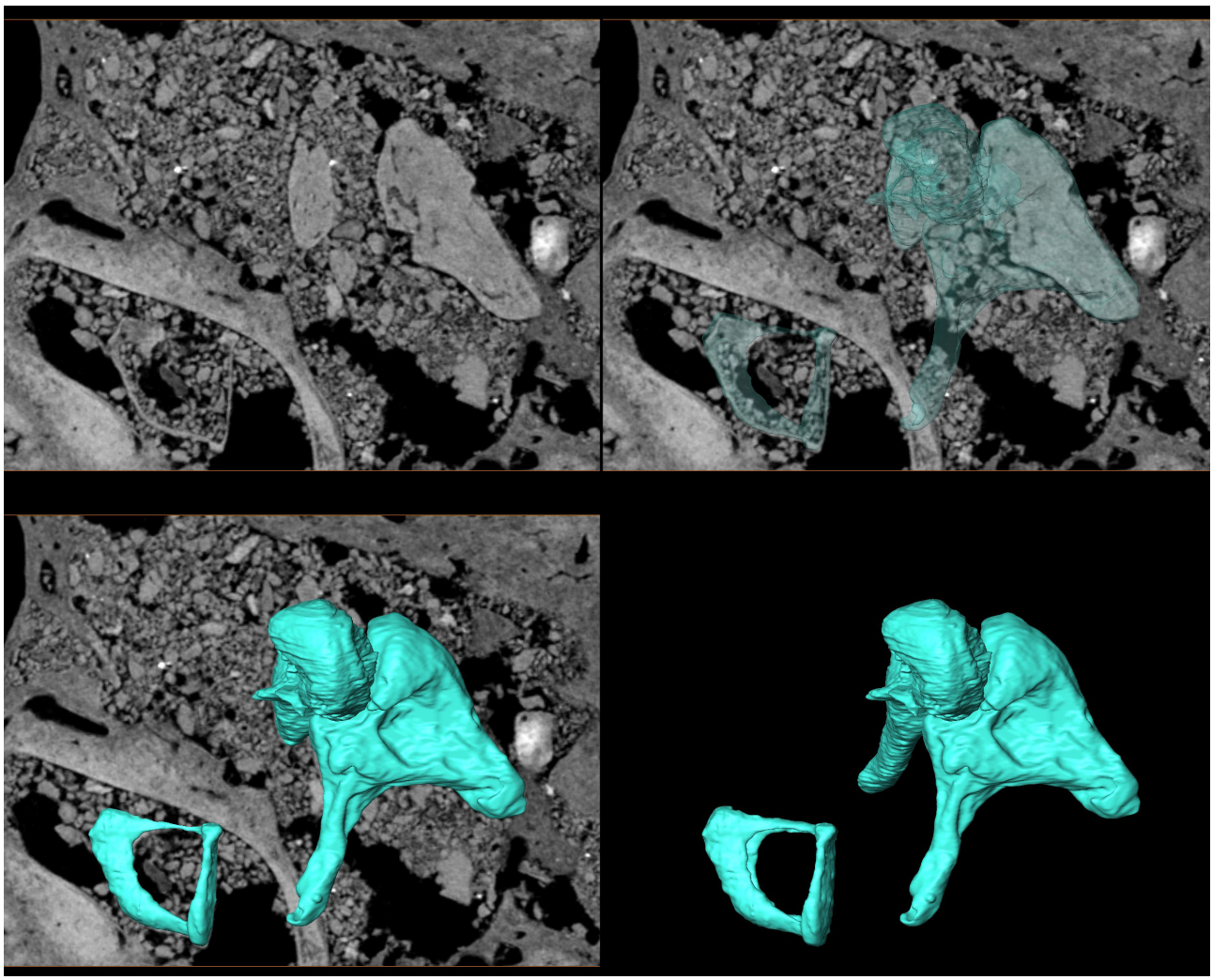

SOM Figure S1. Cross-section of the right temporal bone of La Ferrassie 1 Neandertal showing the position of the three ear ossicles and their 3D virtual reconstructions.

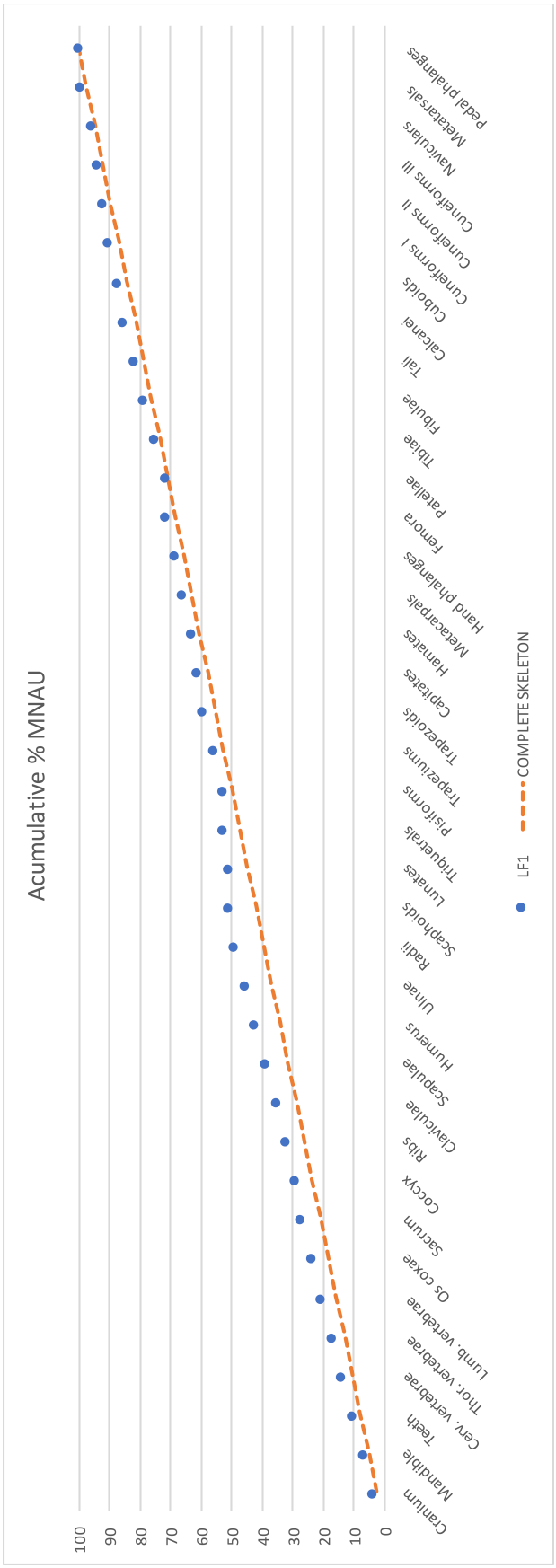

SOM Figure S2. Cumulative percentage of the minimum number of anatomical units (MNAU), i.e., number of bones or bone portions preserved in a sample divided by number of that bone or bone portion in a complete skeleton, present in La Ferrassie 1 (blue dots) compared to what would be expected in a complete skeleton (orange line; see SOM Table S1).

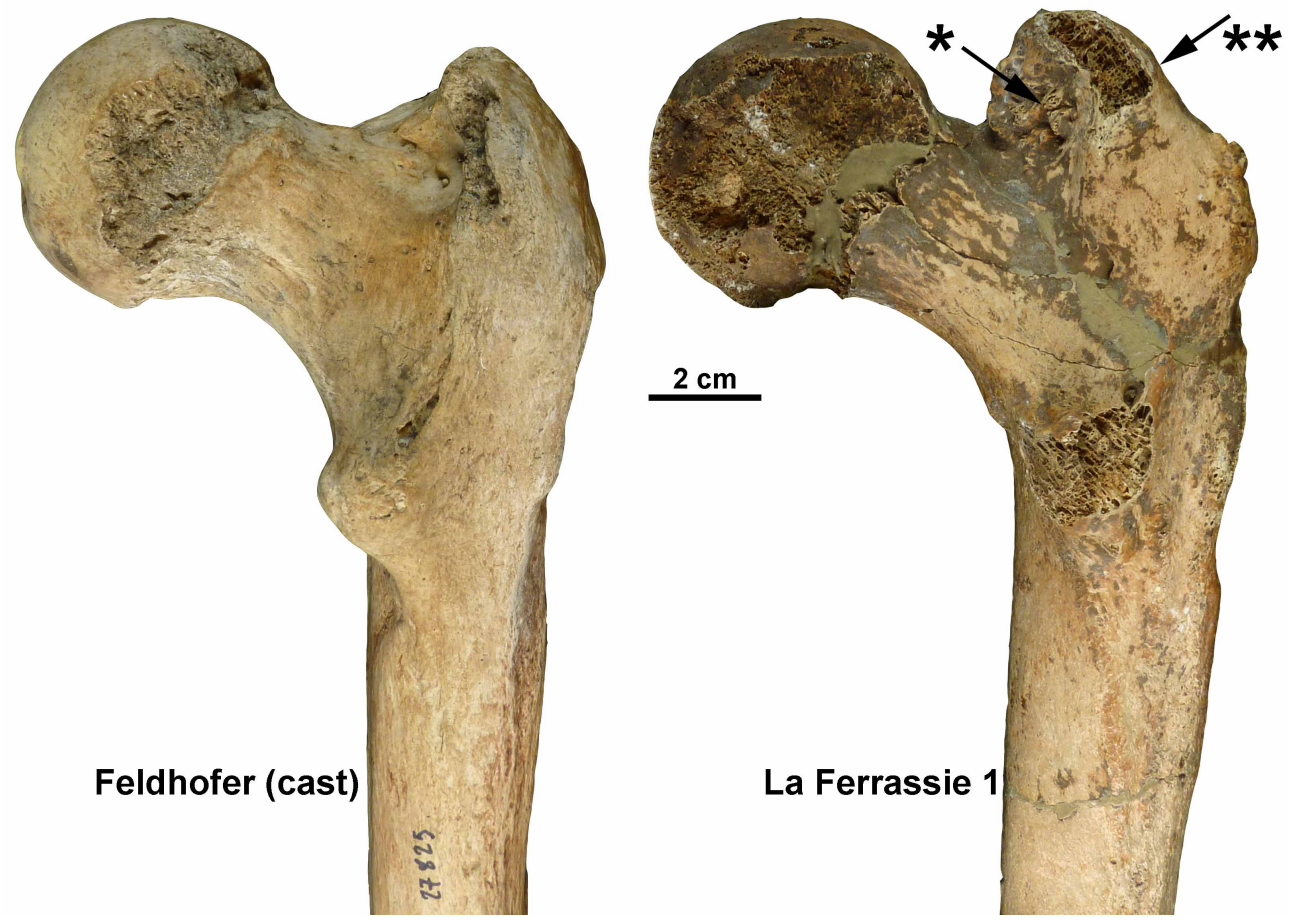

SOM Figure S3. Dorsal view of the cast of the right femur of the Feldhofer Neandertal (left) with the right femur of the La Ferrassie 1 Neandertal. Note the difference in the size and location of the greater trochanter (arrow with **). Note also the exostosis present in the trochanteric fossa (arrow with *).

SOM Figure S4. Left ulna of the La Ferrassie 1 Neandertal skeleton: original bone and 3D reconstruction in ventral (anterior) views (left half of the image) and longitudinal section and detail of the section from the CT-scan showing two natural bone fractures with angles close to 90º (right half of the image).

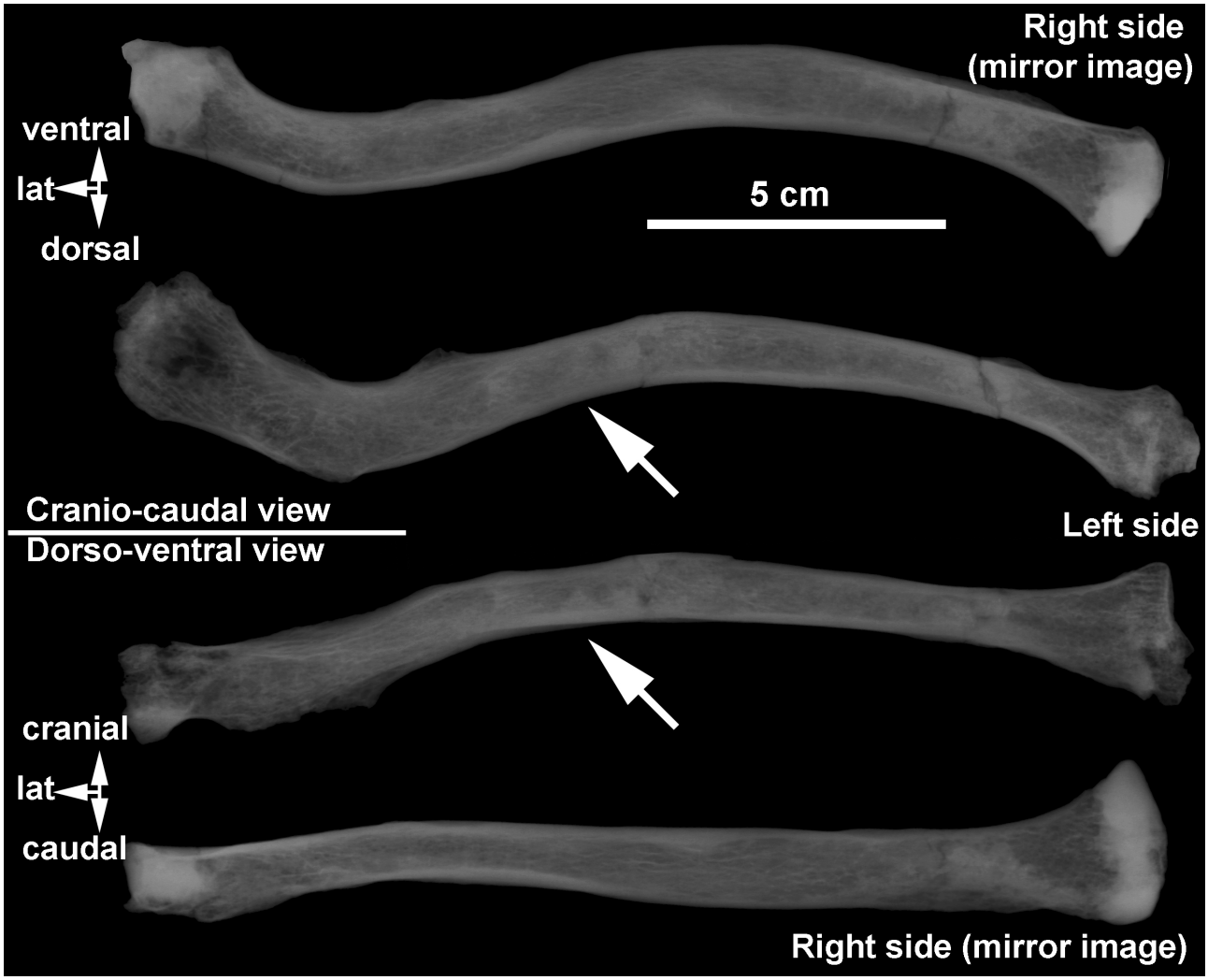

SOM Figure S5. Cranio-caudal and dorso-ventral x-rays of the clavicles of La Ferrassie 1. Note the difference in the trabecular organization in the shaft, which is more irregular in the left clavicle (arrows).

SOM Table S1
Anatomical representation (absolute and relative) of the La Ferrassie 1 individual and cumulative percentage.

Anatomical region	NISP	NME	N°AU	One skeleton	MNAU	Relative MNAU	Cumulative % MNAU
Cranium	>25	1	1	1	1.00	3.41	3.41
Mandible	6	1	1	1	1.00	3.41	6.83
Teeth	32	32	32	32	1.00	3.41	10.24
Cerv. vertebrae	7*	7	7	7	1.00	3.41	13.65
Thor. vertebrae	18*	11	11	12	0.92	3.13	16.78
Lumb. vertebrae	9*	5	5	5	1.00	3.41	20.19
Os coxae	3	2	2	2	1.00	3.41	23.61
Sacrum	3	1	1	1	1.00	3.41	27.02
Coccyx	1	1	1	2	0.50	1.71	28.73
Ribs	43*	22**	22	24	0.92	3.13	31.85
Claviculae	5	2	2	2	1.00	3.41	35.27
Scapulae	7	2	2	2	1.00	3.41	38.68
Humerus	3	2	2	2	1.00	3.41	42.09
Ulnae	4	2	2	2	1.00	3.41	45.51
Radii	3	2	2	2	1.00	3.41	48.92
Scaphoids	1	1	1	2	0.50	1.71	50.63
Lunates	0	0	0	2	0.00	0.00	50.63
Triquetrals	1	1	1	2	0.50	1.71	52.33
Pisiforms	0	0	0	2	0.00	0.00	52.33
Trapeziums	2	2	2	2	1.00	3.41	55.75
Trapezoids	2	2	2	2	1.00	3.41	59.16
Capitates	1	1	1	2	0.50	1.71	60.86
Hamates	1	1	1	2	0.50	1.71	62.57
Metacarpals	16	10	10	10	1.00	3.41	65.98
Hand phalanges	19	18	18	28	0.64	2.19	68.18
Femora	6	2	2	2	1.00	3.41	71.59
Patellae	0	0	0	2	0.00	0.00	71.59
Tibiae	4	2	2	2	1.00	3.41	75.00
Fibulae	5	2	2	2	1.00	3.41	78.42
Tali	2	2	2	2	1.00	3.41	81.83
Calcanei	2	2	2	2	1.00	3.41	85.24
Cuboids	1	1	1	2	0.50	1.71	86.95
Cuneiforms I	2	2	2	2	1.00	3.41	90.36
Cuneiforms II	1	1	1	2	0.50	1.71	92.07
Cuneiforms III	1	1	1	2	0.50	1.71	93.78
Naviculars	1	1	1	2	0.50	1.71	95.48
Metatarsals	15	10	10	10	1.00	3.41	98.89
Pedal phalanges	10	9	9	28	0.32	1.10	100.00

Abbreviations: NISP = Number of Identified Specimens, MNE = Minimum Number of Elements, MNAU = Minimum Number of Anatomical Units, Cumulative % MNAU = Cumulative percentage of the minimum number of anatomical units.

* The vertebrae and ribs are very fragmented. Here we indicate the NISP after all the possible refits were performed.
** Gómez-Olivencia, unpublished data.

SOM Table S2

Comparative sample of ear ossicles used in the present study.

Specimen/Group		Malleus	Incus	Stapes	Oval window	Source
Middle Pleistocene Europe						
	AT-84				X	Martínez et al., 2004
	AT-421				X	Martínez et al., 2004
	AT-667 (Cranium 5)			X	X	Martínez et al., 2004
	AT-3746+3747	X	X			Martínez et al., 2004
	Ehringsdorf H1026	X	X		X	Stoessel et al., 2016a
	Biache-Saint-Vaast 1	X	X			Lisoněk and Trinkaus, 2006; Crevecoeur, 2007
Neandertals						
	La Ferrassie 1	X	X	X		This study
	La Ferrassie 3	X	X	X	X	Quam et al., 2013b
	La Ferrassie 4 bis				X	Quam et al., 2013b
	La Ferrassie 5				X	Quam et al., 2013b
	La Ferrassie 8			X		Gómez-Olivencia et al., 2015
	Subalyuk 2			X		Quam et al., 2013b
	Amud 7		X			Quam and Rak, 2008
	Arcy-sur-Cure				X	Quam et al., 2013b
	Kebara 1				X	Quam et al., 2013b
	Neandertal sample	(n = 4)	(n = 10)	(n = 5)	(n = 13)	Stoessel et al., 2016a
Fossil *H. sapiens*						
	Qafzeh 3				X	Quam et al., 2013b
	Qafzeh 11	X	X		X	Quam and Rak, 2008; Quam et al., 2013b
	Qafzeh 12	X	X		X	Quam and Rak, 2008; Quam et al., 2013b
	Qafzeh 13				X	Quam et al., 2013b
	Qafzeh 15	X	X			Quam and Rak, 2008
	Qafzeh 21		X		X	Quam and Rak, 2008; Quam et al., 2013b
	Skhul 1				X	Quam et al., 2013b
	Border Cave 3				X	Quam et al., 2013b
	Nazlet Khater 2	X				Crevecoeur, 2007
	Pestera cu Oase 2	X		X		Ponce de León and Zollikofer, 2013
	Dolní Věstonice 14	X	X			Lisoněk and Trinkaus, 2006; Quam and Rak, 2008
	Dolní Věstonice 15		X			Lisoněk and Trinkaus, 2006; Quam and Rak, 2008
	Cro-Magnon 1	X	X	X		Stoessel et al., 2016a
	Cro-Magnon 2				X	Quam et al., 2013b
	Abri Pataud 1	X	X			Stoessel et al., 2016a
	Lagar Velho 1	X	X			Quam and Rak, 2008

	Parpalló 1				X	Quam et al., 2013b
Recent *H. sapiens*		(n = 43)	(n = 43)	(n = 40)		Quam and Rak, 2008; Quam et al., 2013b

SOM Table S3
Measurement protocol for the malleus.

No.	Definition	Description
	Orientation	Bone is lying on its posterior aspect (with the articular facet away from the observer) and with the manubrium parallel to the plane of projection, i.e., flat on the surface.
	X-axis (Head/neck axis)	Defined by a line connecting the midpoint of the minimum neck width and the most salient point along the top of the head. This is a slightly different definition than that of Masali (see text).
	Y-axis (Manubrium axis)	Defined by a line connecting the inferiormost points of the short process and the manubrium tip.
1	Total length	Maximum distance from the tip of the manubrium to the top of the head.
2	Manubrium length	Distance from the tip of the short process to the manubrium tip, following the Y-axis.
3	Manubrium M-L thickness	M-L thickness of the manubrium at mid-manubrium length, taken perpendicular to the Y-axis
4	Arc depth of the manubrium	Maximum depth of the curvature of the arc of the manubrium, measured from the point of maximum depth to the Y-axis.
5	Corpus length	Distance from the tip of the head to the lower border of the manubrium, taken following the X-axis.
6	S-I head width	Maximum distance between two parallel lines marking the widest points of the margin of the head, taken perpendicular to the X-axis.
7	Neck width	Minimum distance between the anterior and posterior borders of the neck.
8	Angle between the axes (M)	Angle formed between the X- and Y-axes.
	Manubrium/length index	(Manubrium length/total length)× 100
	Manubrium robusticity index	(Manubrium M-L thickness/manubrium length) × 100
	Manubrium/corpus index	(Manubrium length/corpus length) × 100
	Corpus/length index	(Corpus length/total length) × 100

SOM Table S4
Measurement protocol for the incus.

No.	Definition	Description
	Orientation	Bone is lying on its medial aspect. In this orientation, more of the articular facet is visible and the lowest point of the articular facet is marked by a 'lip'
	X-axis (Long process axis)	Defined by a line joining the tip of the long process to the most salient point along the superior border of the body.
	Y-axis (Short process axis)	Defined by a line joining the tip of the short process to the most salient point along the anterior portion of the superior border of the body.
	Z-axis (Rotational axis)	Defined by a line joining the tip of the short process to the most external point along the margin of the articular facet. This axis approximates the rotational axis of the incus within the tympanic cavity.
9	Short process length	Maximum distance from the tip of the short process to the most salient point along the anterior portion of the superior border of the body, following the Y-axis.
10	Long process length	Maximum distance from the tip of the long process to the most salient point along the superior border of the body.
11	Articular facet height	Maximum height of the articular facet taken perpendicular to the Z-axis.
12	Functional length	Maximum distance from the tip of the long process to the Z-axis, taken perpendicular to the Z-axis.
13	Arc depth of the long process	Maximum depth of the arc along the long process, measured from the plane defined by the lateralmost edge of the articular facet and the lateralmost point along the tip of the long process.
14	Inter-process length	Maximum distance between the most salient points along the superior margin of the short process and the tip of the long process. The lateralmost points of the short and long process tips define the measurement plane.
15	Inter-process arc depth	Maximum depth of the curvature between the short and long crurae tips. The depth is taken perpendicular to the axis defined above for the intercrural length (No. 14).
16	Angle between the axes	Angle formed between the X- and Y-axes.
	Crural index	(Short process length/long process length) × 100

SOM Table S5
Measurement protocol for the stapes.

No.	Definition	Description
	Bone orientation	Bone is lying flat on the surface with the convex (round) side turned toward the observer. This is the "norma craniale" orientation of Masali.
	X-axis (Anterior crus axis)	Defined by a line joining the antero-superior corner of the footplate and the tip of the head.
	Y-axis (Posterior crus axis)	Defined by a line joining the postero-superior corner of the footplate and the tip of the head.
	Z-axis (Footplate axis)	Defined by a line joining the most inferior points along the footplate margin anteriorly and posteriorly.
19	Total height of the Stapes	Maximum height from the lower margin of the footplate to the tip of the head, taken perpendicular to the Z-axis.
20	Head height	Minimum distance between the superior margin of the obturator foramen and the top of the head, taken perpendicular to the Z-axis. The latter point is defined as for total staps height (No. 19).
21	Obturator foramen height	Maximum height of the obturator foramen taken perpendicular to the Z-axis.
22	Obturator foramen width	Maximum width of the obturator foramen taken parallel to the Z-axis.
24	Posterior crus length	Maximum distance from the postero-superior corner of the footplate to the tip of the head, following the Y-axis.
26	Anterior crus length	Maximum distance from the antero-superior corner of the footplate to the tip of the head, following the X-axis.
28	Angle A	Angle between the anterior and posterior crurae, or between the X- and Y-axes.
29	Angle B	Angle between the anterior crus and the footplate, or between the X- and Z-axes.
30	Angle C	Angle between the posterior crus and the footplate, or between the Y- and Z-axes.
31	Footplate length	Maximum length of the footplate.
32	Footplate width	Maximum width of the footplate, not necessarily perpendicular to the length.
33	Footplate area	Measured area of the footplate.
	Stapedial index	(Footplate length/height of the stapes) × 100
	Obturator foramen index	(Obturator foramen width/obturator foramen height) × 100
	Foot plate index	(Footplate width/footplate length) × 100
	Crural index	(Anterior crus length/posterior crus length) × 100

SOM Table S6
Coding for the presence and degree of development of the pathological lesions of the surfaces and edges of both the vertebral body and articular facets[a].

Anatomical region	Code	Description
Subchondral bone (articular facets)	0	Normal
	1	Porosity
	2	Eburnation, destruction of the subchondral surface (porosity), or fusion
Osteophytic lipping (vertebral body and articular surfaces)	0	None
	1	Trace (<1 mm)
	2	Moderate (<4 mm)
	3	Major (>4 mm)
Intervertebral disc surfaces (vertebral bodies)	0	Good condition
	1	Porosity
	2	Schmorl's node, destruction of the subchondral surface (porosity), or eburnation.

[a]Following Dawson and Trinkaus (1997), modified from Bridges (1994).

SOM Table S7

La Ferrassie 1 vertebral pathology from the elements kept in Box 37.

	Anatomical position	C1	C2	C3	C4	C5	C6	C7	T1	T2	T3	T4?	T5-T11	T4?	T9?	T5-T8	T5-T8	T12
	Label*	#a	#b (2)	#d (3)	#c (4)	#e (5)	#f (6)	#g (7)	#h (8)	#i (9)	#j (10)	#k1	#k2	#k3 +#k 4+# k5	#p (13)	#m	#q	#r
Cranial facets	Right surface	0	0	0	0	0	0	0?	0?	0	X						0	X
	Right margin	0?	X	2	2	1	1	X	2	2	X						X	X
	Left surface	0	0	1	0	0	0	0	0	0	0		0				X	X
	Left margin	0?	1?	2	2	2	2	1	2	2	X		1				X	X
Caudal facets	Right surface	0	0	0	0	0	0	0	0	0	0						0	X
	Right margin	X	2	2	2	2	2	2	X	1	X						X	X
	Left surface	0	1	0	0	0	0	0	0	0	X			1	0		0	0
	Left margin	1	3	1	2	2	1	1	X	X	X			1	1		X	2?
Cranial body	Surface	-	-	0	0	0	0	X	X	0	X	0?				X	X	0?
	Ventral	-	-	1?	X	X	X	X	X	X	X	X				X	X	X
	Dorsal	-	-	0	0	X	0	X	X	X	0?	0				1	X	X
	Right	-	-	1?	X	X	X	X	X	X	X	X				X	X	X
	Left	-	-	1?	X	0	1?	X	X	X	X	X				X	X	0
Caudal body	Surface	-	0	0	0	0	0	0?	0	0	0?	0?				X	X	0?
	Ventral	-	X	X	0?	0?	X	X	X	1?	X	X				X	X	X
	Dorsal	-	1	0	1	1	1	1	1	1	1	0				2	1	1
	Right	-	1?	0	1	X	X	X	X	1?	1?	X				X	X	X
	Left	-	1?	0	1	X	X	X	X	1?	1?	X				X	X	0?
Costal facets (vertebral body)	Right surface								X	X	X	0				0	X	X
	Right margin								X	X	X	X				X	X	X
	Left surface								X	X	0	0				0	0	0
	Left margin								X	X	X	0				X	X	2
Costal facets (transverse process)	Right surface								X	0	0							-
	Right margin								X	X	X							-
	Left surface								X	X	X							-
	Left margin								X	X	X							-

*Following Gómez-Olivencia, 2013.

Subchondral bone: 0 = normal; 1 = porosity; 2 = eburnation, destruction of the subchondral surface (porosity), or fusion.

Osteophytic lipping: 0 = none; 1 = trace (<1 mm); 2 = moderate (<4 mm); 3 = major (>4 mm).

Intervertebral disc surfaces: 0 = good condition; 1 = porosity; 2 = Schmorl's node, destruction of the subchondral surface (porosity), or eburnation**.**

SOM Table S8

La Ferrassie 1 vertebral pathology from the elements kept in Box 38.

	Anatomical position	T7-T8?	T9	T	L1?	L3?	L2	L3	L4	L5
	Label	#z	#s1	#s2	#t2	#x	#aa (21)	#ab (22)	#ad (23)	#ac (24)
Cranial facets	Right surface		X	0					0	0?
	Right margin		X	1					1	X
	Left surface		X	X				0	0	0-1
	Left margin		X	X				X	1	2
Caudal facets	Right surface		X	X				0	0	0
	Right margin		X	X				1	1	1-2
	Left surface		X	X			0	0	0	0
	Left margin		X	X			2	3	3	2
Cranial body	Surface	0?	X	X	X	0-1				
	Ventral	X	X	X	2	2				
	Dorsal	1	X	X	X	0				
	Right	X	X	X	X	3				
	Left	X	X	X	X	X				
Caudal body	Surface	X	0?	X	0?	0				
	Ventral	X	X	X	X	X				
	Dorsal	2	0	X	0	0				
	Right	X	X	X	2	1				
	Left	X	X	X	X	1+				
Costal facets (vertebral body)	Right surface	X	0	X						
	Right margin	1	X	X						
	Left surface	X	0?	X						
	Left margin	X	0?	X						

Subchondral bone: 0 = normal; 1 = porosity; 2 = eburnation, destruction of the subchondral surface (porosity), or fusion.
Osteophytic lipping: 0 = none; 1 = trace (<1 mm); 2 = moderate (<4 mm); 3 = major (>4 mm).
Intervertebral disc surfaces: 0 = good condition; 1 = porosity; 2 = Schmorl's node, destruction of the subchondral surface (porosity), or eburnation.

SOM Table S9

Evidences of scoliosis in the LF1 spine.

Physical label	Virtual label[a]	Anatomical position	Vertebral body (larger side)[b] (Right/Left)	Articular pillar/mass (larger side) (Right/Left)	Spinous process twisting (in cranial view)	Rotation of the spinous process (in dorsal view)[c]
	#a	C1	X	-	X	X
2	#b	C2	-	R (Left pathologically remodelled)		
3	#d	C3	L (15.0/17.0)	R (Left pathologically remodelled) (8.5/6.4)	L (~7º)	Broken spinous process
4	#c	C4	-	R (13.5/11.0)	R (~8º)	
5	#e	C5	-	L (9.9/11.3)	Straight	No rotation
6	#f	C6	-	= (12.4/12.4)	Straight	No rotation
7	#g	C7	-	-	R (~8º)	
8	#h	T1	-	R ((30.2)/28.2)	R (~7º)	Clockwise (?). Tip missing.
9	#i	T2	R (17.3/16.5)	R (36.4/(34.0))	R (~5º)	Clockwise (~10º). Tip missing.
10	#j	T3	-	-	-	-
11	#k1	T4?	-			
11	#k3+#k4	T4?			R	Clockwise (?)
14	#q	T7			Straight?	No rotation (?)
19	#r	T12	= (23.7/24.0)	-	-	-
	#x	L3?	L (22.6/25.7)			
22	#ab	L3	-	L (based on the crcd larger lower left facet)	-	Clockwise (?)
23	#ad	L4	-	R (48.6/(48.0)) Left side pathologically remodelled	L (~3º)	-
24	#ac	L5	-	-	Straight?	Clockwise (~20-25º)

[a]Following Gómez-Olivencia, 2013.

[b]In cervical vertebrae, it refers to the development of the uncinate processes.

[c]No rotation refers to a rotation degree of <5º.

X=This anatomical region does not exist in this vertebra.

- = Not possible to assess, due to preservation.

In the cervical vertebrae, the thickness of the articular pillars has been measured from the inferior surface (positioning the caliper parallel to the orientation of the facet), to the middle of the upper facet.

In thoracic and lumbar vertebrae, we have measured the bi-articular diameter, i.e., from the cranialmost point of the upper articular facet to the caudalmost point of the inferior articular facet.

SOM Table S10

Absolute values[a] and percentage asymmetry[b] for the clavicular curvatures in cranial and dorsal views

Specimen	Species	Cranial view						Dorsal view					
		Internal curvature			External curvature			Inferior curvature			Superior curvature		
		R	L	% asym.	R	L	% asym.	R	L	% asym.	R	L	% asym.
La Ferrassie 1	*H. neanderthalensis*	13.2	12.3	7.3	14.2	17.7	24.6	5.4	8.2	51.8	5.8	2.6	123.1
Kebara 2	*H. neanderthalensis*	11.3	11.1	1.8	9.5	16.5	73.7	3.4	4.9	44.1	0.0	0.0	0.0
Regourdou 1	*H. neanderthalensis*	10.0	11.9	19.0	14.5	13.2	9.8	7.4	3.0	146.7	8.0	3.2	150.0
KNM-WT 15000	*Homo erectus*	13.1	15.3	16.8	14.6	14.7	0.7	5.0	5.3	6.0	7.4	8.1	9.5

R = Right; L = Left; asym. = asymmetry.

[a]Values from Voisin (2006).

[b]Calculated following Franciscus and Churchill, 2002.

References

Bridges, P.S., 1994. Vertebral arthritis and physical activities in the prehistoric Southeastern United States. Am. J. Phys. Anthropol. 93, 83–93.

Crevecoeur, I., 2007. New discovery of an Upper Paleolithic auditory ossicle: The right malleus of Nazlet Khater 2. J. Hum. Evol. 52, 341–345.

Dawson, J.E., Trinkaus, E., 1997. Vertebral osteoarthritis of the La Chapelle-aux-Saints 1 Neanderthal. J. Archaeol. Sci. 24, 1015–1021.

Franciscus, R.G., Churchill, S.E., 2002. The costal skeleton of Shanidar 3 and a reappraisal of Neandertal thoracic morphology. J. Hum. Evol. 42, 303–356.

Gómez-Olivencia, A., 2013. The presacral spine of the La Ferrassie 1 Neandertal: a revised inventory. Bull. Mém. Soc. Anthropol. Paris 25, 19–38.

Gómez-Olivencia, A., Crevecoeur, I., Balzeau, A., 2015. La Ferrassie 8 Neandertal child reloaded: New remains and re-assessment of the original collection. J. Hum. Evol. 82, 107–126.

Lisoněk, P., Trinkaus, E., 2006. The auditory ossicles. In: Trinkaus, E., Svoboda, J. (Eds.), Early Modern Human Evolution in Central Europe: The People of Dolní Věstonice and Pavlov. Oxford University Press, Oxford, pp. 153–155.

Martínez, I., Arsuaga, J.-L., Quam, R., Lorenzo, C., Gracia, A., Carretero, J.-M., Rosa, M., Jarabo, P., Carbonell, E., Bermúdez De Castro, J.-M., 2004. Auditory capacities in Middle Pleistocene humans from the Sierra de Atapuerca in Spain. Proc. Natl. Acad. Sci. USA 101, 9976–9981.

Ponce de León, M., Zollikofer, C.P.E., 2013. The internal cranial morphology of Oase 2. In: Trinkaus, E., Constantin, S., Zilhão, J. (Eds.), Life and Death at the Pestera cu Oase. A Setting for Modern Human Emergence in Europe, pp. 332–347.

Quam, R., Rak, Y., 2008. Auditory ossicles from southwest Asian Mousterian sites. J. Hum. Evol. 54, 414–433.

Quam, R., Martínez, I., Arsuaga, J.L., 2013. Reassessment of the La Ferrassie 3 Neandertal ossicular chain. J. Hum. Evol. 64, 250–262.

Stoessel, A., David, R., Gunz, P., Schmidt, T., Spoor, F., Hublin, J.-J., 2016a. Morphology and function of Neandertal and modern human ear ossicles. Proc. Natl. Acad. Sci. USA 113, 11489–11494.

Voisin, J.-L., 2006. Krapina and other neanderthal clavicles: a peculiar morphology? Period. Biol. 108, 331–339.